Journal of Mass Spectrometry and Advances in the Clinical Lab 24 (2022) 80–89

Contents lists available at ScienceDirect

Journal of Mass Spectrometry and Advances in the Clinical Lab

journal homepage: www.sciencedirect.com/journal/journal-of-mass-spectrometry-and-advances-in-the-clinical-lab

Research Article

Towards real-time intraoperative tissue interrogation for REIMS-guided glioma surgery

Laura Van Hese [a,b], Steven De Vleeschouwer [c], Tom Theys [c], Emma Larivière [c], Lien Solie [c], Raf Sciot [d], Tiffany Porta Siegel [a], Steffen Rex [b], Ron M.A. Heeren [a], Eva Cuypers [a,*]

[a] Maastricht MultiModal Molecular Imaging (M4I) Institute, Division of Imaging Mass Spectrometry, Maastricht University, 6229 ER Maastricht, The Netherlands
[b] Department of Anaesthesiology, UZ Leuven; Department of Cardiovascular Sciences, KU Leuven, 3000 Leuven, Belgium
[c] Department of Neurosurgery, Laboratory for Experimental Neurosurgery and Neuroanatomy, UZ Leuven, KU Leuven, 3000 Leuven, Belgium
[d] Department of Pathology, University Hospitals Leuven, KU Leuven, 3000 Leuven, Belgium

ARTICLE INFO

Keywords:
REIMS
Real-time characterisation
Brain tumors
Tumor margin delineation

ABSTRACT

Introduction: The main goal of brain tumour surgery is to maximize tumour resection while avoiding neurological deficits. Accurate characterization of tissue and delineation of resection margins are, therefore, essential to achieve optimal surgical results.
Objectives: The primary objective of this study was to develop and validate a mass spectrometry- based technique for the molecular characterization of high- and low-grade glioma tissue during surgery.
Methods: An electrosurgical knife is connected to a mass spectrometer (iKnife). Using this system, an aerosol created during electrosurgical resection is aspirated to a mass spectrometer to determine the molecular profile of the tissue within seconds. This rapid evaporative ionization mass spectrometry (REIMS) technique is used to create a chemical profile database and develop a real-time tissue recognition system based on machine learning.
Results: Classification models were built by analysing biopsies from 36 patients who underwent brain tumour resection. Our multivariate statistical model could differentiate between astrocytoma grade II and III, glioblastoma, oligodendroglioma grade II and III, and normal brain tissue with an 88% overall accuracy. Astrocytoma and oligodendroglioma grade II were separated from normal brain with a 96% correct classification rate. REIMS could differentiate between different percentages of GBM with 99.2% sensitivity and different percentages of astrocytoma grade II with 97.5% sensitivity.
Conclusion: Real-time information during electrosurgical dissection can improve intra-operative decision-making, leading to a more accurate tumour removal for different glioma subtypes.

Introduction

Gliomas are the most common primary brain tumours and, according to the National Institutes of Health (NIH), represent about 81% of malignant brain lesions [1]. The clinical management of these tumours remains a significant challenge due to their biological behaviour, their infiltration in the viable and functioning brain, and close proximity to critical functional brain tissue [2]. Accurate characterization of tissue and delineation of resection margins is essential to maximize tumour resection and minimize postoperative neurological deficits. Currently, histopathological grading of surgical biopsies and genetic phenotyping determines first-line treatment. However, these results are usually only available after the surgery has finished.

Intraoperative tissue diagnosis, in particular with respect to the determination of tumour type and grade, is mostly limited to frozen section analyses. This approach relies on haematoxylin and eosin (H&E) staining of cellular structures to reveal morphologic and cytologic features. The interpretation of the results is mainly subjective, based on the trained eye and experience of the pathologist. However, the genetic variability and genomic instability of brain tumours remains invisible under a microscope. Furthermore, histopathology is time-consuming (20–30 mins) and costly and, therefore, rarely used in practice [3]. Significant progress has been made in the development of medical imaging modalities and brain-mapping techniques, such as magnetic resonance imaging, computed tomography or fluorescence-guided surgery (using 5-aminolevulinic acid; 5-ALA) [4,5]. These approaches provide an insight into the location and extent of the brain tumour and

* Corresponding author at: M4I Institute, Division of Imaging Mass Spectrometry, Universiteitssingel 50, 6229 ER Maastricht, The Netherlands.
E-mail address: e.cuypers@maastrichtuniversity.nl (E. Cuypers).

https://doi.org/10.1016/j.jmsacl.2022.04.004
Received 22 November 2021; Received in revised form 27 April 2022; Accepted 27 April 2022
Available online 29 April 2022

Nomenclature

5-ALA	5-aminolevulinic acid
AMX	Abstract Model Builder
BMI	Body Mass Index
CUSA/SSI	Cavitron ultrasonic surgical aspiration/sonic spray ionisation
FA	Fatty acids
FN	False negative
FP	False positive
GBM	Glioblastoma
H&E	Haematoxylin and eosin
LDA	Linear discriminant analyses
MRI	Magnetic resonance imaging
NIH	National Institutes of Health
PA	Phosphatidic acids
PCA	Principal component analyses
PE	Phosphatidylethanolamines
QTOF	Quadrupole time-of-flight
REIMS	Rapid evaporative ionization mass spectrometry
SP	Sphingolipids
TIC	Total ion chromatogram
TN	True negative
TP	True positive
WHO	World Health Organisation

into the relationship between the tumour cells and the surrounding tissue. For the resection of high-grade gliomas, 5-ALA is a well-established intraoperative adjunct to differentiate tumour from the surrounding brain parenchyma. However, at the margin of these diffusely infiltrating glioma tumours the fluorescence gradually becomes weak and therefore difficult to judge relative to the nonfluorescent normal tissue. Besides, the lack of fluorescence does not equate to a complete absence of tumour, especially in the peritumoral regions [6–9]. Furthermore, in low-grade gliomas, the use of 5-ALA remains limited due to lack of fluorescence in a large percentage of patients.

Currently, fluorescence-guided surgery with 5-ALA is often used in combination with intraoperative contrast-enhanced magnetic resonance imaging (MRI) to determine the resection margin in high-grade gliomas [10]. However, the MRI appearance of high-grade gliomas does not always correspond to their histopathological composition, often restricting the identification of tumour to contrast-enhanced areas and making characterisation of the areas of infiltrative tumour unreliable [11]. Here, a precise correlation between the preoperative imaging data and the patient's brain anatomy is crucial to guarantee an accurate localisation of the tumour during surgery. Currently, this correlation is strongly influenced by brain shift or the intraoperative deformation of brain tissues. Therefore, the correlation of brain structures in preoperative and intraoperative images becomes inaccurate, and reduces the precision by which resection margins, based on in vivo imaging alone, can be determined [12]. Preoperative localisation of these tumours using conventional medical imaging showed an increased probability for successful treatment. However, in up to 65–80% of glioma resections, some residual tumour tissue remains after surgery. Up to now, surgeons still suffer from the lack of intraoperative feedback, especially in low-grade gliomas, that provides guidance towards accurate identification of, not only the residual tumour tissue, but also the proximity to the surrounding normal tissue [13].

Electrosurgical (electro-cauterisation) devices are used during virtually every surgical resection of a brain lesion in order to achieve haemostasis and an improved accuracy of dissection. A major by-product is 'smoke', which results from evaporating tissue debris during electrosurgical procedures. This smoke has already been shown to contain a rich source of molecular information that allows recognition and delineation of pathological tissue in real-time using mass spectrometry [14–17]. The technique, called rapid evaporative ionization mass spectrometry (REIMS), connects an electrosurgical knife to a mass spectrometer (a so-called intelligent knife, or iKnife), converting tissue components into gas-phase ionic species appropriate for mass spectrometric analysis [18]. Furthermore, the procedure of sampling the smoke, transfer to the mass spectrometer, analysis and feedback to the surgeon takes just 0.7–2.5 s, without specialized sample preparation. Similar sampling techniques hyphenated to mass spectrometry have already shown potential for the in-depth characterisation of brain tumours. However, most of these techniques, such as the MasSpec Pen [19], SpiderMass [20,21], and cavitron ultrasonic surgical aspiration/sonic spray ionisation (CUSA/SSI) [22] only allow sampling of biopsies, and cannot be used for guiding tissue resection [23].

Real-time tissue interrogation during electrosurgical dissection could lead to more accurate tumour removal based on instantly available information on the nature of the tissue. In this project, we further developed and validated the use of the REIMS technique for real-time characterisation of gliomas. Here, we determined the applicability of REIMS to differentiate between the different types and grades of gliomas, as well as measure the diagnostic accuracy and sensitivity of REIMS to detect tumour cells in the tumour margin of both high- and low-grade gliomas.

Materials and methods

Biological samples

All patients (>11 years of age) were scheduled to undergo an elective neurosurgical procedure under total intravenous general anaesthesia. This single-centre, prospective observational study was performed at Leuven University hospitals, Gasthuisberg (Leuven, Belgium). The study protocol was approved by the Ethics Committee Research UZ/KU Leuven (S60291) and the project was registered under the UZ Leuven Tissue Bank. Thirty-six patients were enrolled and provided written informed consent prior to participation. Patients were included when resection of brain tissue had to be performed in the context of their underlying disease, independent of the current study. While part of the brain tissue was sent to the pathology department for histopathological evaluation, the remainder was used for ex vivo REIMS analysis.

Demographic and clinicopathological data included age, gender, height, Body Mass Index (BMI) and post-operative histopathological information (including histological tumour subtype (astrocytoma, oligodendroglioma and glioblastoma (GBM)); and WHO grade). Where feasible, for GBM, tissue was provided from the centre of the tumour and from the infiltrating tumour margin. As a control, tissue from the temporal neocortex was obtained from patients undergoing mesial temporal epilepsy surgery. All samples were immediately stored at −80 °C until analysis.

Patients suspected to harbour malignant gliomas were all operated under 5-ALA induced fluorescence-guided resections: sampling in these tumours was always performed in the bright fluorescence zones for bulky tumour parts and in the fluorescence margin zones for invasion fronts.

Sample processing with REIMS

REIMS analyses were performed directly on the thawed brain samples. All investigated samples had one freeze–thaw cycle. Based on the size of the tissue biopsy, 1 to 5 cuts were made using a monopolar

electrosurgical pencil with needle electrode (Ø 2.8 mm) (Covidien, Medtronic, Jette, Belgium) in pure cut setting (continuous RF wave) with a Covidien Force FX™ generator (Medtronic, Jette, Belgium). Furthermore, a supplementary video (Supplementary Data 2) shows application of the bipolar forceps (Covidien Medtronic, Jette, Belgium) in coagulation mode for the classification of human brain tumours. The power settings ranged between 20 and 25 Watts. The aerosol resulting from electrosurgical dissection was aspirated using a Venturi pump and transferred to the mass spectrometer using a tygon evacuation tube. Mass spectrometric analysis was performed using a Waters Xevo G2-XS quadrupole time-of-flight (QTOF) instrument equipped with a REIMS source (Waters Corporation, Wilmslow, UK). In addition, the aerosol was mixed with isopropanol as the matrix solvent during measurement, prior to introduction into the REIMS source, to enhance the signal intensity of the ions and obtain a constant cleaning source. A flow rate ranging from 0.15 to 0.20 mL/min was investigated and the best signal intensity was obtained at 0.20 mL/min. Leucine enkephalin (0.15 ng/μL) was used as an external lock mass (mass in negative mode m/z 554.2615) for all samples. The sample cone and heater bias were set to 80 V. All analyses were performed in negative ionisation mode over a range of 50–1000 m/z and with a scan time of 1 sec. Prior to every use, the instrument was calibrated using sodium formate.

Histopathology

Prior to and following sample processing using REIMS on the GBM tissue samples, the samples were sectioned at 12 μm on a cryotome (Leica) for histopathology of the tissue that was burnt using the iKnife. H&E stained sections were scanned using an Aperio CS2 pathology scanner (Leica®). Subsequently, H&E-stained slides were examined by a senior expert histopathologist to identify the area surrounding the sampling point and assign a tissue diagnosis. This provided the best possible knowledge and insight about the tissue under study in lieu of the complete tissue removal at the REIMS analysis points.

For low-grade gliomas, multiple REIMS mass spectra were obtained and compared to evaluate the reproducibility of the REIMS technique. Supplementary Data 1, Fig. 1, shows the spectra obtained from two REIMS 'burning' points in one astrocytoma GR II sample and in one oligodendroglioma GR II sample. In both low-grade glioma's, similar mass spectra were obtained from both analysis points, showing a good reproducibility of REIMS analyses in low-grade gliomas.

Data analysis

MassLynx MS software (Waters Corporation, Wilmslow, UK) was applied for mass spectrometric data acquisition. Abstract Model Builder (AMX, Version 0.9.2092.0, Waters Research Centre, Hungary) was used to process all raw mass spectrometric data collected on the REIMS instrument, model building and model classification. REIMS mean mass spectra were summed for each burn to create a single profile per sampling spot. For each model, all spectra were binned with a bin of 0.5 m/z and a mass range of m/z 300 to 900. Lock mass correction, background subtraction and normalisation (divided by the ion chromatogram (TIC)) was performed to pre-process the spectra prior to building the model.

Multivariate statistical analyses, i.e. principal component analyses (PCA) and linear discriminant analyses (LDA), were performed on the defined REIMS spectra. Fragmentation patterns were not taken into account for these statistical analyses and were only used for lipid identification purposes. Unsupervised PCA is a method for dimensionality reduction, because smaller data sets are easier to evaluate and visualize. This allows one to obtain insights into the variance in the lipid patterns that are included in this model. Furthermore, supervised LDA was performed to further model and optimize the differences between the classes of data. PCA/LDA classification, based on the REIMS lipid patterns, was compared with the histopathological evaluation of the tissue to calculate the accuracy of the REIMS based classifier. Cross-validation of the LDA models was performed using leave-20%-out cross-validation, which randomly selects 20% of the spectra in one round to leave it out of the training set and builds the model on the remaining 80%. Loading plots were generated to identify spectral differences between the different brain tumour types and grades and between tumour and normal tissue. Furthermore, PCA/LDA models created in the AMX software were exported into the recognition software used in post-processing and real-time mode for the direct characterisation of blind samples.

From the generated confusion matrix, the performance was evaluated based on true positive (TP), false positive (FP), false negative (FN), true negative (TN) using the following:

$$\text{Sensitivity} = \frac{\text{TP}}{\text{TP} + \text{FN}}$$

$$\text{Specificity} = \frac{\text{TN}}{\text{TN} + \text{FP}}$$

Lipid identification

Lipid identification was based on the data acquired from REIMS and on the exact mass measurement acquired using MALDI-based DDA [24]. A MALDI/ESI Injector (Spectroglyph LLC, Kennewick, WA) is coupled to an Orbitrap Elite using the earlier described DDA-imaging method by Ellis et al. [24]. Furthermore, REIMS MS/MS fragmentation patterns were used to confirm the lipid identification. REIMS tandem MS was performed using the Xevo G2-XS QTOF mass spectrometer by collision-induced dissociation with argon gas. The obtained exact masses and MS/MS data from the Orbitrap Elite mass spectrometer and fragmentation patterns from REIMS tandem MS were compared to the online LIPIDMAPS structure database, the ALEX 123 lipid database, the Human Metabolome Database and reference literature. GraphPad (version 8) was used for the analyses of patient metadata and for the analyses of the raw data matrix exported from AMX software.

Mathematical models for classification accuracy

The classification accuracy of REIMS for GBM and astrocytoma GR II, was evaluated by creating two mathematical models. The raw mass spectra of either all GBM and normal brain samples or all astrocytoma GR II and normal brain samples, obtained by REIMS, were exported from AMX model builder to CVS. In turn, the spectra of the diseased samples (GBM or astrocytoma GRII) were combined with the spectra of the normal control brain samples in order to create different percentages of "disease". Every sample point in a percentage class consisted of 100 spectra and one percentage class consisted of ten sampling points. For instance, the 70% GBM class, consists of ten sample points that are all built out of the combined spectra from 70 GBM samples and the spectra from 30 normal brain samples.

Results

A total of 36 specimens from adult neurosurgical patients were included (23 men and 13 women), including 3 diffuse astrocytomas (WHO grade II), 3 anaplastic astrocytomas (WHO grade III), 11 glioblastomas (WHO grade IV), 6 oligodendrogliomas (WHO grade II), 2 anaplastic oligodendrogliomas (WHO grade III) and 11 control samples. The demographic data of all patients are presented in Supplementary Data 1, Table 1. Depending on the biopsy size, 1 to 5 analysis points per sample produced a total of 124 mass spectra (Normal = 31, Astrocytoma grade II = 10, Astrocytoma grade III = 30, GBM = 27, Oligodendroglioma grade II = 17, Oligodendroglioma grade III = 9).

REIMS classification of the different types and grades of glioma brain tumours

Tumour identification within a timeframe of seconds could significantly influence surgical decisions. Using REIMS, the direct intraoperative identification of tumour type and grade could guide and influence the surgical strategy in real-time. Therefore, a PCA/LDA classification model was built including the following classes; Normal brain tissue, Astrocytoma grade II, Astrocytoma grade III, GBM, Oligodendroglioma grade II and Oligodendroglioma grade III, to allow a rapid overall differentiation between the different types and grades of glioma brain tumours (Fig. 1a). Data from 124 sampling points from a total of 36 individual specimens were used; i.e. from 13 normal specimens (31 sampling points) and 27 tumour specimens (93 sampling points). The leave-20%-out cross-validation of this model resulted in an overall accuracy of 87.90%, allowing a good first classification (Fig. 1c).

REIMS Tandem MS and DDA experiments were performed to identify the lipids that significantly differed between the classes (Fig. 1b). Online MS databases were used for lipid identification based on the fragmentation and the accurate mass data. Mass peaks that contributed to the class separation were mainly glycerophospholipids with phosphatidylethanolamines (PE) being the most commonly identified. Furthermore, phosphatidic acids (PA), sphingolipids (SP) and fatty acids (FA) were also identified (Table 1).

Interestingly, these differences between the classes were represented by changing ratios of these mass peaks rather than the presence or absence of specific lipid species. Glioblastomas were separated with a 100% correct classification rate from other glioma subtypes along the first linear discriminant (LD1). However, in this case, only sampling points originating from bulk tumour were taken into account. Furthermore, 30% of the low-grade gliomas were incorrectly classified as normal brain tissue in this model.

The applicability of this model was also tested using a bipolar forceps, since these are commonly used during the main part of brain surgery. A GBM sample and normal brain tissue sample were subjected to REIMS analysis using the bipolar forceps in coagulation mode. The recognition software was concordant with the histopathological assessment of these samples. An illustrative video can be found in Supplementary Data 2. While it was only tested on a limited number of samples, our results indicate that the model built using the monopolar

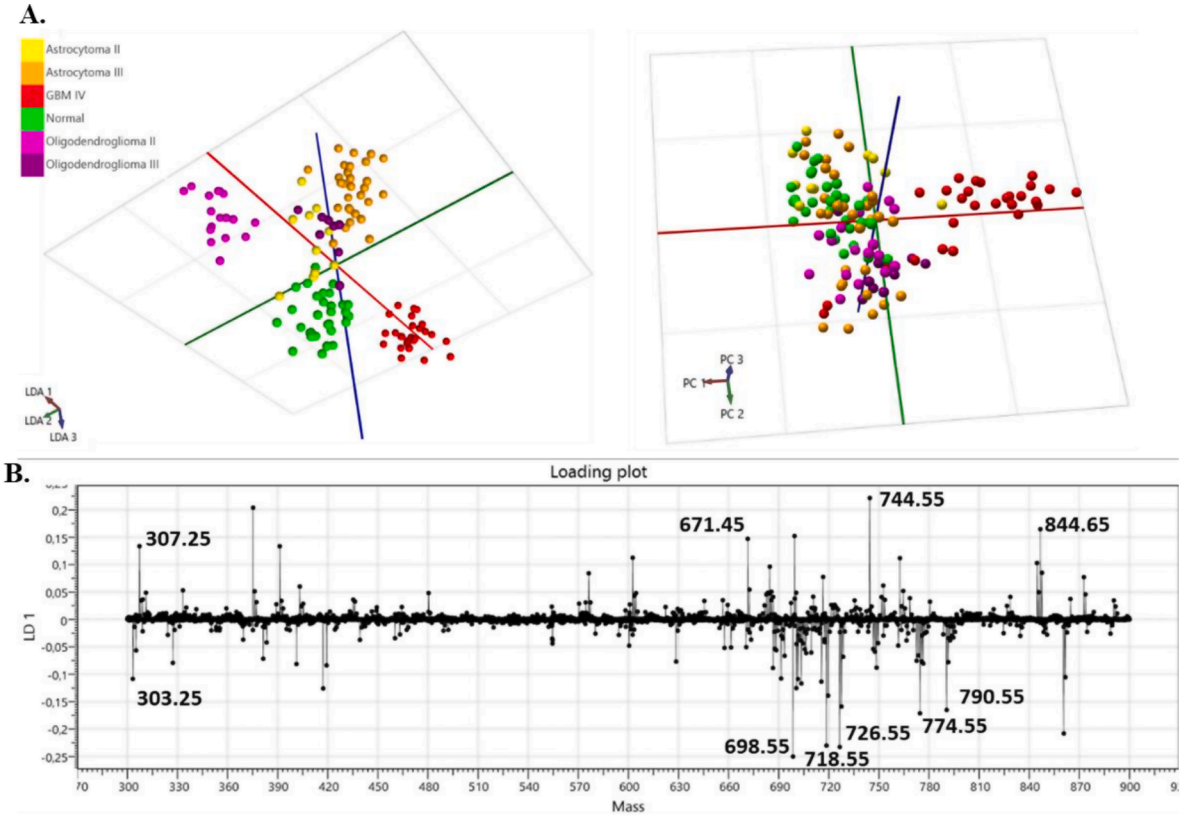

C.

Overall accuracy 87.90%		Predicted Class (%)					
		Astrocytoma II	Astrocytoma III	GBM	Normal	Oligodendroglioma II	Oligodendroglioma III
Actual Class (%)	Astrocytoma II	**60**	0	0	30	0	10
	Astrocytoma III	4	**83**	0	0	0	13
	GBM	0	0	**100**	0	0	0
	Normal	0	0	3	**90**	0	7
	Oligodendroglioma II	0	0	0	0	**100**	0
	Oligodendroglioma III	0	22	0	11	0	**67**

Fig. 1. Multivariate statistical analysis of different glioma types. A 3D PCA/LDA classification model obtained ex vivo of 5 different types and grades of glioma vs control brain tissue. **B** The first loading plot for glioma and normal brain tissue demonstrates the contribution of the ten lipids. C Leave 20%-out cross-validation, proportion (%) of correct classification following PCA/LDA analysis.

Table 1
Lipid assignments by tandem mass spectrometry (MS/MS) for the ten most relevant peaks contributing to the LDA class separation between intra-axial brain tumours and normal brain tissue.

Model	m/z	Lipid class	Configuration	Ion
Intra-axial brain tumours vs Normal	303.25	Fatty acyl	FA 20:4	[M – H]⁻
	307.25	Fatty acyl	FA 20:2	[M – H]⁻
	671.45	Phosphatidic acid	PA 16:0_18:2 and PA 16:1_18:1	[M – H]⁻
	698.55	Phosphatidic acid	PA 16:0_20:2 and PA 18:1_18:1	[M – H]⁻
	718.55	Phosphatidyl-ethanolamine	PE 16:0_18:0	[M – H]⁻
	726.55	Phosphatidyl-ethanolamine	PE O-36:3	[M – H]⁻
	744.55	Phosphatidyl-ethanolamine	PE 16:0_20:1 and PE 18:0_18:1	[M – H]⁻
	774.55	Phosphatidyl-ethanolamine	PE O-18:1_22:6	[M – H]⁻
	790.55	Phosphatidyl-ethanolamine	PE 18:0_22:6	[M – H]⁻
	844.65	Phosphatidylserine	PS 18:1_22:0 and 18:1_22:1	[M – H]⁻

needle electrode could also be applied using bipolar forceps.

REIMS classification accuracy in high-grade glioma

During high-grade glioma resection, the invasive tumour margin between tumour tissue and the surrounding brain is still difficult to visualise. While significant advancements have been made in the technologies of neurosurgery, none of these provide the required molecular precision to delineate / evaluate tumour margins and the extent of infiltration. Therefore, we evaluated the sensitivity of REIMS in the prediction of this tumour margin (percentage of brain tumour that can be detected). A PCA/LDA model was built with different percentages of GBM (Fig. 2a). Each class was mathematically built by combining GBM and control brain tissue spectral data from 100 sampling points into the following percentage classes: 0%, 1%, 2%, 3%, 4%, 5%, 10%, 20%, 30%, 40%, 50%, 60%, 70%, 80%, 90% and 100% GBM. Lock mass correction, background subtraction and normalisation (divided by the total ion chromatogram (TIC)) were performed to pre-process the spectra prior to building the model.

The leave-20%-out cross validation showed an overall correct classification rate of 97.04%, a sensitivity of 99.3% and a specificity of 100% (Fig. 2b). With up to 1% GBM in the investigated sample, there is a 20 % chance of a false negative result with this model. This model showed a 100% correct classification rate starting from 5% GBM. Furthermore, the accuracy of this percentage model was tested by exporting the model data into the AMX recognition software. Here, three REIMS spectra originating from the bulk tumour, fluorescent margin region and normal brain tissue were analysed (Fig. 3a). These samples were evaluated as an independent validation set and were not used to build the model in Fig. 2a. The spectra obtained from the bulk tumour and control brain tissue were classified as 100% GBM and 0% GBM, respectively. In the spectrum originating from the invasive region 10% GBM was detected.

In order to validate these results, the recognition output was

A.

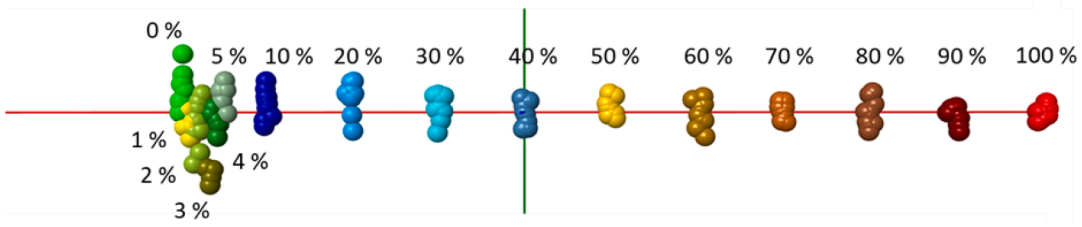

B.

Overall accuracy 97.04%		Predicted Class (%)															
		0	1	2	3	4	5	10	20	30	40	50	60	70	80	90	100
Actual Class (%)	0	100	0	0	0	0	0	0	0	0	0	0	0	0	0	0	0
	1	20	60	20	0	0	0	0	0	0	0	0	0	0	0	0	0
	2	0	20	80	0	0	0	0	0	0	0	0	0	0	0	0	0
	3	0	0	0	100	0	0	0	0	0	0	0	0	0	0	0	0
	4	0	0	0	0	80	20	0	0	0	0	0	0	0	0	0	0
	5	0	0	0	0	0	100	0	0	0	0	0	0	0	0	0	0
	10	0	0	0	0	0	0	100	0	0	0	0	0	0	0	0	0
	20	0	0	0	0	0	0	0	100	0	0	0	0	0	0	0	0
	30	0	0	0	0	0	0	0	0	100	0	0	0	0	0	0	0
	40	0	0	0	0	0	0	0	0	0	100	0	0	0	0	0	0
	50	0	0	0	0	0	0	0	0	0	0	100	0	0	0	0	0
	60	0	0	0	0	0	0	0	0	0	0	0	100	0	0	0	0
	70	0	0	0	0	0	0	0	0	0	0	0	0	100	0	0	0
	80	0	0	0	0	0	0	0	0	0	0	0	0	0	100	0	0
	90	0	0	0	0	0	0	0	0	0	0	0	0	0	0	100	0
	100	0	0	0	0	0	0	0	0	0	0	0	0	0	0	0	100

Fig. 2. Classification model of different percentages of GBM. A PCA/LDA model of different % of GBM using the mean spectral information of 100 GBM and control brain tissue REIMS spectra; **B** Leave-20%-out cross-validation, proportion (%) of correct classification following PCA/LDA analysis.

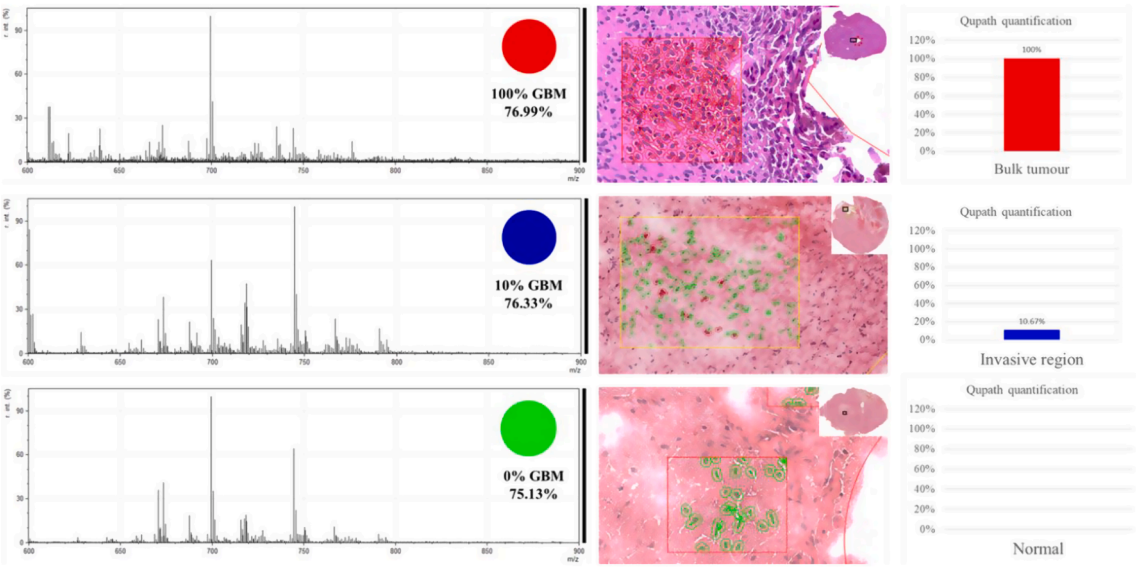

Fig. 3. Validation of the REIMS technique for GBM cells A. REIMS mass spectra obtained from the bulk tumour in the fluorescent margin of the tumour and in a control brain sample. These REIMS spectra were further used in the recognition software for identification with the classification model described in Fig. 2a. **B.** Histological image (H&E); full tissue section in the upper right corner and magnification of the highlighted region (black square) after cell detection and classification. **C.** The Qupath quantification of the proportion of tumoral cells in the selected areas representative for the area of the REIMS 'burning point'.

compared to the actual percentages of tumour cells quantified in the H&E slides of the same tissue sample after REIMS cauterisation. This was done by analysing the scanned H&E images in Qupath (v0.2.3), [25] an open source software developed for digital pathology image annotation and analysis [26]. Here, in an independent set of H&E GBM samples, regions of tumour and normal brain tissue were manually defined (Fig. 3b). Automated cell detection, based on morphometric features of the detected cells, was used to train a classifier with the ability to distinguish between tumour and normal cells. This classifier was then applied to an area representative of the area of the REIMS 'burning

A.

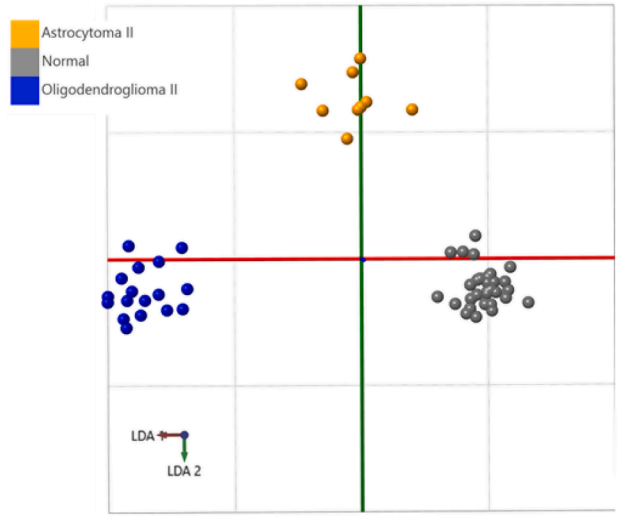

B.

	Overall Accuracy 96.49%	Predicted Class (%)		
		Astrocytoma II	Oligodendroglioma II	Normal
Actual Class (%)	Astrocytoma II	**77.78%**	0%	22.22%
	Oligodendroglioma II	0%	**100%**	0%
	Normal	0%	0%	**100%**

Fig. 4. Multivariate statistical analysis of low-grade gliomas. A 3D PCA/LDA model of astrocytoma GII and oligodendroglioma GII vs normal brain tissue. **B** Leave-20%-out cross-validation, proportion (%) of correct classification following PCA/LDA analysis.

point'. Here, the edges of the burning point were avoided to prevent the inclusion of cells with changed morphology due to the cauterisation process common with REIMS. Application of this method affirmed 100% and 0% of the tumour cells in the bulk tumour and normal tissue samples, respectively. Furthermore, in the tissue sample originating from the fluorescent margin, Qupath quantification resulted in 10.67% GBM cells (Fig. 3c). This real-time, intra-operative information on the percentage of remaining tumour cells in the tumour margin provides the neurosurgeon with crucial and previously unavailable information, which could improve patient outcome.

REIMS classification accuracy of low-grade glioma

Similar to high-grade gliomas, the visual discrimination between tumour and normal brain in low-grade gliomas remains challenging. Low-grade gliomas are slowly evolving, but highly invasive tumours that show only subtle differences versus the surrounding functioning brain. Furthermore, our first classification model (Fig. 1) showed a relatively high percentage of low-grade gliomas that were incorrectly classified as normal brain tissue. Therefore, we created a classification model consisting solely of low-grade gliomas to in order to increase the classification rate of these tumours (Fig. 4a). A PCA/LDA model was created based on data from 57 sampling points; i.e. from 6 oligodendroglioma grade II (17 sampling points), 3 astrocytoma grade II (9 sampling points) and 11 normal specimens (31 sampling points). The leave-20%-out cross-validation resulted in an overall accuracy of 96.49%, with a false negative rate of 6% and a false positive rate of 0% (Fig. 4b). Oligodendroglioma grade II was separated from normal brain tissue along the first linear discriminant with 100% correct classification rate. Twenty-two percent of the astrocytoma grade II sampling points were wrongly classified as normal brain tissue.

Therefore, the accuracy of this technique for the separation of astrocytoma grade II and normal brain was tested in more detail by using a percentage model of increasing percentage of astrocytoma grade II. This model was built in the same way as the previous GBM % model and showed an overall accuracy of 75%, a sensitivity of 97.5% and a specificity of 50% (Fig. 5). At 1% astrocytoma grade II there is a 20% chance the model gives a false negative result and at 3% astrocytoma grade II there is a 10%. Furthermore, until 2% astrocytoma grade II, there is a 30% change the model shows a false positive result. These results demonstrate that REIMS can serve as an easy-to-use, real-time, intra-operative detection technique for residual low-grade glioma tumour tissue. REIMS might, therefore, significantly influence surgical decision making, allowing maximal extent of resection in low-grade gliomas.

Discussion

The introduction of analytical technologies, such as MRI, ultrasound, neuro-navigation and, in malignant gliomas, fluorescence-guided surgery, supports the surgeon to identify tumour tissue intra-operatively and delineate a perceived margin. Nevertheless, these techniques show limited chemical information, sometimes low sensitivity and often the need for the use of contrast agents or pre-operative administration of (pro-)drugs. These issues create the need for a rapid and accurate

A.

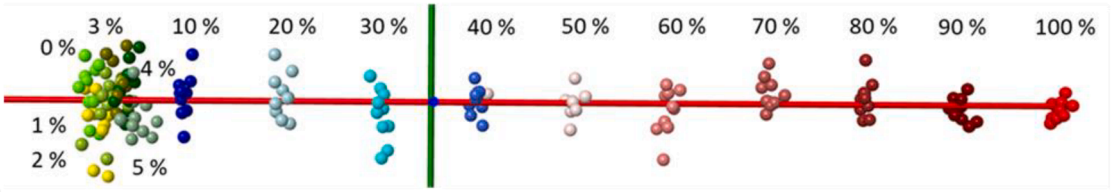

B.

Overall accuracy (75%)		Predicted class (%)															
		0	1	2	3	4	5	10	20	30	40	50	60	70	80	90	100
Actual class (%)	0	50	20	30	0	0	0	0	0	0	0	0	0	0	0	0	0
	1	20	20	50	10	0	0	0	0	0	0	0	0	0	0	0	0
	2	0	20	30	20	30	0	0	0	0	0	0	0	0	0	0	0
	3	10	0	30	40	20	0	0	0	0	0	0	0	0	0	0	0
	4	0	0	20	30	30	20	0	0	0	0	0	0	0	0	0	0
	5	0	0	20	10	30	40	0	0	0	0	0	0	0	0	0	0
	10	0	0	0	0	0	0	100	0	0	0	0	0	0	0	0	0
	20	0	0	0	0	0	0	0	100	0	0	0	0	0	0	0	0
	30	0	0	0	0	0	0	0	0	100	0	0	0	0	0	0	0
	40	0	0	0	0	0	0	0	0	0	100	0	0	0	0	0	0
	50	0	0	0	0	0	0	0	0	0	10	90	0	0	0	0	0
	60	0	0	0	0	0	0	0	0	0	0	0	100	0	0	0	0
	70	0	0	0	0	0	0	0	0	0	0	0	0	100	0	0	0
	80	0	0	0	0	0	0	0	0	0	0	0	0	0	100	0	0
	90	0	0	0	0	0	0	0	0	0	0	0	0	0	0	100	0
	100	0	0	0	0	0	0	0	0	0	0	0	0	0	0	0	100

Fig. 5. Classification model of different percentages of astrocytoma GII. A PCA/LDA model of different % of astrocytoma GII built using the mean spectral information of 100 astrocytoma GII and normal brain tissue REIMS spectra; **B** Leave-20%-out cross-validation, proportion (%) of correct classification following PCA/LDA analysis.

characterisation method of brain tumours and their margins without interfering with the surgical workflow. Our work investigates the feasibility, accuracy and sensitivity of a mass spectrometric based diagnostic approach for the differentiation of gliomas, both low-grade and high-grade, from the surrounding healthy and functional brain.

The visualisation of the invasive margin of gliomas and the assessment of the status of post-resection cavity walls is challenging for the surgeon. Currently, intraoperative MRI and 5-ALA-based fluorescence are the only tools in clinical routine that show residual tumour in situ. At the margin of high-grade gliomas, 5-ALA has been shown to label tumour with a 91% sensitivity and 80% specificity, compared to a 66% sensitivity and 60% specificity with intraoperative MRI [27]. However, the diagnostic accuracy is based on histological evaluation of these techniques, causing results to be highly dependent on the trained-eye and expertise of the pathologist. REIMS could provide a more sensitive platform to characterize the disease state and its borders by identifying changes in the molecular profile of the tissue. Our model, built to differentiate different percentages of GBM and normal brain tissue, showed a 97% correct classification rate and could differentiate different percentages of GBM from normal brain with 99.3% sensitivity and 100% specificity. A recent study by Molina et al. investigated the diagnostic accuracy and perception of protoporphyrin IX discrimination using a novel filter system with higher background illumination compared to the gold standard filter system [28]. Notwithstanding these improvements, they still found a median tumour cell density of 13% in the non-fluorescent marginal tissue. Therefore, REIMS could complement 5-ALA fluorescence during the resection of high-grade gliomas and provide a more objective insight in the margins of fluorescence.

Notably, the intensity of fluorescence of 5-ALA depends on the grade and molecular characteristics of the tumour, as well as on the pharmacokinetic features of the patient. In almost half of the patients, the fluorescence is perceived as suboptimal [29,30]. However, expertise of the surgeon might also influence this outcome. The intra-operative evaluation of the different shades of fluorescence is subjective and strongly depends on the experience of the neurosurgeon. Lastly, the administration of 5-ALA harbours the risk of photosensitivity. The proposed REIMS technology does not require the use of pro-drugs and tissue classification results are presented in a standardized, universal, and easily interpretable format.

The importance of marginal, and maybe supramarginal, resection is not exclusive for high-grade gliomas. In low-grade glioma, a growing body of evidence also supports the positive prognostic impact of maximized resection on progression-free survival. Here, the role of 5-ALA fluorescent guided surgery remains limited, because visible fluorescence is only observed in 10–20% of patients [31,32]. Therefore, intraoperative and post-operative MRI are considered the gold standard in the follow-up and further management of low-grade gliomas, the former being expensive, time consuming and not real-time. Post-operative MRI is used to detect tumour remnants and, therefore, has a strong influence on the adjuvant therapy. However, due to the silent progress of the disease and the ability to infiltrate brain tissue beyond MRI boundaries, it is, up to now, almost not possible to detect complete tumour extension of low-grade glioma tumours [33,34]. Furthermore, since most of these tumours are non-enhancing, the estimation of residual tumour cells after surgery remains challenging [35]. In this study, we developed a REIMS based classification system that can differentiate between low-grade astrocytoma, low-grade oligodendroglioma and normal brain tissue with a 96.49% correct classification rate. Furthermore, to obtain insight into the accuracy of REIMS for low-grade gliomas, a classification model was built to differentiate between percentages of grade II astrocytoma. This model only showed false negative results up to 5% grade II astrocytoma cells and showed a 80% correct classification rate starting from 10% grade II astrocytoma. In turn, REIMS would allow real-time differentiation between tumour cells and normal cells in the margin of these slowly infiltrating tumours and even provide information on the amount of tumour cells in the resected tissue. Furthermore, the REIMS technique will allow detection of the complete range of biomolecules, including biomarkers, such as proteins and lipids.

For this project, an electrosurgical needle (2 mm) was used instead of an electrosurgical blade to increase the reproducibility of our REIMS analyses [23]. REIMS is a destructive process and, therefore, it is impossible to have histopathological confirmation of the exact cellular content under analysis. To minimise this uncertainty as much as possible, the electrosurgical needle was used and a frozen tissue section was made before and after REIMS analyses of the GBM samples. Furthermore, needle ablation has been widely applied to neurosurgery compared to the use of an electrosurgical blade. Therefore, we expect that our ex vivo results will be easily translated to in vivo use. The limitation of using an electrosurgical needle compared to an electrosurgical knife is the decreased amount of smoke and subsequent lower intensity mass spectrum.

For REIMS, a recognition software has already been developed to automatically analyse the REIMS spectra. In a next step, this technique will be implemented in the operating theatre. The equipment is transportable and can be easily moved between the different operating rooms. The system consists of an analysis device (iKnife connected to a mass spectrometer), a computer with mass spectrometry analysis software to automatically analyse the REIMS spectra and an indication screen for the neurosurgeon. This screen shows a fast and clear indication of the type, grade and/or cell percentage of the tumour. The depicted information is based on the databases and PCA/LDA analyses we created in this research using the REIMS set-up. Importantly, in the operating room, it is expected that a monitor will directly provide the surgeon with a fast and clear diagnostic result, without the need for any mass spectrometric training. Furthermore, this technique has already proven its ability in real-time tumour margin detection and phenotyping [36,37]. Balog et al. evaluated a REIMS endoscopic method in vivo on three patients referred for colonoscopy. Here, a uniform spectral pattern was found and colonic polyps could be differentiated from the healthy mucosal layer, in agreement with the ex vivo studies [37]. Vaysse et al. recently evaluated the applicability of REIMS to use breast stromal molecular information to guide breast conserving surgery [16]. They showed that a REIMS model of ex vivo molecular profiles enabled in vivo recognition of stroma and, thereby, illustrated the usability of an ex vivo created model during surgery. Furthermore, a combination of REIMS and DESI might provide complementary information in the characterisation of brain tumours. DESI-MS allows the acquisition of images of the tissue, providing a correlation of chemical and spatial information. Theoretically, similar chemical species are observed by DESI and REIMS. However, the spectral profiles obtained are still markedly different. In order to solve this challenge, previous work suggested a cross-platform normalisation approach in order to convert the raw mass spectra obtained by the different ionisation methods [38]. This might allow one to use different ionisation methods for the population of future large scale MS-based tissue datasets.

For neurosurgeons engaged in oncological surgery, this technique could potentially represent a step towards the next level in terms of intra-operative assessment of extent of resection, both for low- and high-grade gliomas. The technology allows a continuous and rapid (0.7–2.5 s) sampling option for the resected tissue, barely interfering with the normal surgical workflow and with high spatial and temporal resolution. With ongoing resection of tumour invasion zones, it is anticipated according to our model, that REIMS sampling results will show degressive percentages of tumour presence in the surrounding normal brain, thereby delivering the first method that would be able to quantify extent of resection in invasive tumour areas.

Our results indicate that REIMS is a real-time, reliable methodology that can be implemented in the current surgical workflow for brain tumour removal. However, a limitation of this study is the limited sample sizes for the different classifications. Therefore, the prediction values only provide a valuable estimate of the prediction performance. A follow-up study with a larger sample set will be required in order to

further validate these results. We demonstrate the complexity and heterogeneity of glioma infiltration and confirm the utility and potential of REIMS in the characterisation of the tumour and the tumour margins within seconds. To date, unresected residual tumour is still the leading cause of recurrence and tumour progression and extent of resection is an independent prognosticator for both low- and high-grade gliomas. Here, REIMS coupled with intraoperative imaging techniques and functional monitoring tools will maximize tumour resection and avoid post-operative neurological deficits and ultimately improve patient outcome.

Funding

This work was supported by the FWO research foundation, Belgium (PhD fellowship strategic basic research: 1S87718N), by the FWO research foundation, Belgium (TBM (Applied Biomedical Research with a Primary Social finality) projects: T001919N), the clinical research and education council (KOOR) of UZ Leuven, Belgium and with the support of the Dutch Province of Limburg through the LINK program.

CRediT authorship contribution statement

Laura Van Hese: Conceptualization, Methodology, Investigation, Formal analysis, Visualization, Writing – original draft, Writing – review & editing. **Steven De Vleeschouwer:** Conceptualization, Methodology, Resources, Writing – review & editing. **Tom Theys:** Conceptualization, Methodology, Resources, Writing – review & editing. **Emma Larivière:** Resources. **Lien Solie:** Resources. **Raf Sciot:** Formal analysis, Visualization, Writing – review & editing. **Tiffany Porta Siegel:** Conceptualization, Methodology, Formal analysis, Visualization, Writing – review & editing. **Steffen Rex:** Conceptualization, Methodology, Writing – review & editing, Writing – review & editing. **Ron M.A. Heeren:** Conceptualization, Methodology, Formal analysis, Visualization, Writing – review & editing. **Eva Cuypers:** Conceptualization, Methodology, Investigation, Formal analysis, Visualization, Writing – original draft, Writing – review & editing.

Declaration of Competing Interest

The authors declare that they have no known competing financial interests or personal relationships that could have appeared to influence the work reported in this paper.

Acknowledgements

The authors would like to gratefully acknowledge the help from the neurosurgeons at UZ Leuven, Belgium for providing tissue samples. We are grateful to Julia Balog (Waters Research Centre) and Steve Pringle (Waters Corporation) for their technical support with the REIMS-Xevo system.

Appendix A. Supplementary data

Supplementary data to this article can be found online at https://doi.org/10.1016/j.jmsacl.2022.04.004.

References

[1] F. Hanif, K. Muzaffar, K. Perveen, S.M. Malhi, S.U. Simjee, Glioblastoma Multiforme: a review of its epidemiology and pathogenesis through clinical presentation and treatment, Asian Pac. J. Cancer Prev. 18 (2017) 3–9, https://doi.org/10.22034/APJCP.2017.18.1.3.

[2] N.Y.R. Agar, A.J. Golby, K.L. Ligon, I. Norton, V. Mohan, J.M. Wiseman, A. Tannenbaum, F.A. Jolesz, Development of stereotactic mass spectrometry for brain tumor surgery, Neurosurgery 68 (2011) 280–290, https://doi.org/10.1227/NEU.0b013e3181ff9cbb.

[3] D. Calligaris, I. Norton, D.R. Feldman, J.L. Ide, I.F. Dunn, L.S. Eberlin, R.G. Cooks, F.A. Jolesz, A.J. Golby, S. Santagata, N.Y. Agar, Mass spectrometry imaging as a tool for surgical decision-making, J. Mass Spectrom. 48 (2013) 1178–1187, https://doi.org/10.1002/jms.3295.

[4] S. Cha, Update on brain tumor imaging: from anatomy to physiology, Am. J. Neuroradiol. 27 (2006) 475 LP – 487. http://www.ajnr.org/content/27/3/475.abstract.

[5] W. Stummer, S. Stocker, S. Wagner, H. Stepp, C. Fritsch, C. Goetz, A.E. Goetz, R. Kiefmann, H.J. Reulen, Intraoperative detection of malignant gliomas by 5-aminolevulinic acid-induced porphyrin fluorescence, Neurosurgery 42 (1998) 516–518, https://doi.org/10.1097/00006123-199803000-00017.

[6] N.B. Dadario, D. Khatri, N. Reichman, C.D. Nwagwu, R.S. D'Amico, 5-Aminolevulinic acid–shedding light on where to focus, World Neurosurgery 150 (2021) 9–16.

[7] I.W.H. Chung, S. Eljamel, Risk factors for developing oral 5-aminolevulinic acid-induced side effects in patients undergoing fluorescence guided resection, Photodiagnosis Photodyn. Ther. 10 (2013) 362–367, https://doi.org/10.1016/j.pdpdt.2013.03.007.

[8] D.W. Roberts, P.A. Valdés, B.T. Harris, K.M. Fontaine, A. Hartov, X. Fan, S. Ji, S. S. Lollis, B.W. Pogue, F. Leblond, T.D. Tosteson, B.C. Wilson, K.D. Paulsen, Coregistered fluorescence-enhanced tumor resection of malignant glioma: relationships between δ-aminolevulinic acid-induced protoporphyrin IX fluorescence, magnetic resonance imaging enhancement, and neuropathological parameters, J. Neurosurg. 114 (2011) 595–603, https://doi.org/10.3171/2010.2.JNS091322.

[9] P.P. Panciani, M. Fontanella, B. Schatlo, D. Garbossa, A. Agnoletti, A. Ducati, M. Lanotte, Fluorescence and image guided resection in high grade glioma, Clin. Neurol. Neurosurg. 114 (2012) 37–41, https://doi.org/10.1016/j.clineuro.2011.09.001.

[10] W. Stummer, U. Pichlmeier, T. Meinel, O.D. Wiestler, F. Zanella, H.-J. Reulen, Fluorescence-guided surgery with 5-aminolevulinic acid for resection of malignant glioma: a randomised controlled multicentre phase III trial, Lancet Oncol. 7 (2006) 392–401, https://doi.org/10.1016/S1470-2045(06)70665-9.

[11] O. Eidel, S. Burth, J.-O. Neumann, P.J. Kieslich, F. Sahm, C. Jungk, P. Kickingereder, S. Bickelhaupt, S. Mundiyanapurath, P. Bäumer, W. Wick, H.-P. Schlemmer, K. Kiening, A. Unterberg, M. Bendszus, A. Radbruch, Tumor infiltration in enhancing and non-enhancing parts of glioblastoma: a correlation with histopathology, PLoS ONE 12 (2017), e0169292, https://doi.org/10.1371/journal.pone.0169292.

[12] S. Bayer, A. Maier, M. Ostermeier, R. Fahrig, Intraoperative imaging modalities and compensation for brain shift in tumor resection surgery, Int. J. Biomed. Imaging. 2017 (2017) 6028645, https://doi.org/10.1155/2017/6028645.

[13] S. Hu, H. Kang, Y. Baek, G. El Fakhri, A. Kuang, H.S. Choi, Real-time imaging of brain tumor for image-guided surgery, Adv. Healthc. Mater. 7 (2018), e1800066, https://doi.org/10.1002/adhm.201800066.

[14] J. Balog, L. Sasi-Szabo, J. Kinross, M.R. Lewis, L.J. Muirhead, K. Veselkov, R. Mirnezami, B. Dezso, L. Damjanovich, A. Darzi, J.K. Nicholson, Z. Takats, Intraoperative tissue identification using rapid evaporative ionization mass spectrometry, Sci. Transl. Med. 5 (2013) 194ra93–194ra93. 10.1126/scitranslmed.3005623.

[15] J. Balog, T. Szaniszlo, K.-C. Schaefer, J. Denes, A. Lopata, L. Godorhazy, D. Szalay, L. Balogh, L. Sasi-Szabo, M. Toth, Z. Takats, Identification of biological tissues by rapid evaporative ionization mass spectrometry, Anal. Chem. 82 (2010) 7343–7350, https://doi.org/10.1021/ac101283x.

[16] P.-M. Vaysse, L.F.S. Kooreman, S.M.E. Engelen, B. Kremer, S.W.M. Olde Damink, R. M.A. Heeren, M.L. Smidt, T. Porta Siegel, Stromal vapors for real-time molecular guidance of breast-conserving surgery, Sci. Rep. 10 (2020) 20109, https://doi.org/10.1038/s41598-020-77102-1.

[17] P.-M. Vaysse, H.I. Grabsch, M.F.C.M. van den Hout, M.H.A. Bemelmans, R.M. A. Heeren, S.W.M. Olde Damink, T. Porta Siegel, Real-time lipid patterns to classify viable and necrotic liver tumors, Lab. Investig. 101 (2021) 381–395, https://doi.org/10.1038/s41374-020-00526-w.

[18] K.-C. Schafer, J. Denes, K. Albrecht, T. Szaniszlo, J. Balog, R. Skoumal, M. Katona, M. Toth, L. Balogh, Z. Takats, In vivo, in situ tissue analysis using rapid evaporative ionization mass spectrometry, Angew. Chem. Int. Ed. Engl. 48 (2009) 8240–8242, https://doi.org/10.1002/anie.200902546.

[19] J. Zhang, J. Rector, J.Q. Lin, J.H. Young, M. Sans, N. Katta, N. Giese, W. Yu, C. Nagi, J. Suliburk, J. Liu, A. Bensussan, R.J. DeHoog, K.Y. Garza, B. Ludolph, A. G. Sorace, A. Syed, A. Zahedivash, T.E. Milner, L.S. Eberlin, Nondestructive tissue analysis for ex vivo and in vivo cancer diagnosis using a handheld mass spectrometry system, Sci. Transl. Med. 9 (2017), https://doi.org/10.1126/scitranslmed.aan3968.

[20] B. Fatou, P. Saudemont, E. Leblanc, D. Vinatier, V. Mesdag, M. Wisztorski, C. Focsa, M. Salzet, M. Ziskind, I. Fournier, In vivo real-time mass spectrometry for guided surgery application, Sci. Rep. 6 (2016) 25919, https://doi.org/10.1038/srep25919.

[21] B. Fatou, P. Saudemont, M. Duhamel, M. Ziskind, C. Focsa, M. Salzet, I. Fournier, Real time and in vivo pharmaceutical and environmental studies with SpiderMass instrument, J. Biotechnol. 281 (2018) 61–66, https://doi.org/10.1016/j.jbiotec.2018.06.339.

[22] K.-C. Schäfer, J. Balog, T. Szaniszló, D. Szalay, G. Mezey, J. Dénes, L. Bognár, M. Oertel, Z. Takáts, Real time analysis of brain tissue by direct combination of ultrasonic surgical aspiration and sonic spray mass spectrometry, Anal. Chem. 83 (2011) 7729–7735, https://doi.org/10.1021/ac201251s.

[23] M. Genangeli, R.M.A. Heeren, T. Porta Siegel, Tissue classification by rapid evaporative ionization mass spectrometry (REIMS): comparison between a diathermic knife and CO2 laser sampling on classification performance, Anal.

Bioanal. Chem. 411 (2019) 7943–7955, https://doi.org/10.1007/s00216-019-02148-8.
[24] S.R. Ellis, M.R.L. Paine, G.B. Eijkel, J.K. Pauling, P. Husen, M.W. Jervelund, M. Hermansson, C.S. Ejsing, R.M.A. Heeren, Automated, parallel mass spectrometry imaging and structural identification of lipids, Nat. Methods 15 (2018) 515–518, https://doi.org/10.1038/s41592-018-0010-6.
[25] K. Ščupáková, F. Dewez, A.K. Walch, R.M.A. Heeren, B. Balluff, Morphometric cell classification for single-cell MALDI-mass spectrometry imaging, Angew. Chem. Int. Ed. 59 (2020) 17447–17450, https://doi.org/10.1002/anie.202007315.
[26] P. Bankhead, M.B. Loughrey, J.A. Fernández, Y. Dombrowski, D.G. McArt, P. D. Dunne, S. McQuaid, R.T. Gray, L.J. Murray, H.G. Coleman, J.A. James, M. Salto-Tellez, P.W. Hamilton, QuPath: Open source software for digital pathology image analysis, Sci. Rep. 7 (2017) 16878, https://doi.org/10.1038/s41598-017-17204-5.
[27] J. Coburger, J. Engelke, A. Scheuerle, D.R. Thal, M. Hlavac, C.R. Wirtz, R. König, Tumor detection with 5-aminolevulinic acid fluorescence and Gd-DTPA-enhanced intraoperative MRI at the border of contrast-enhancing lesions: a prospective study based on histopathological assessment, Neurosurg. Focus. 36 (2014) E3, https://doi.org/10.3171/2013.11.FOCUS13463.
[28] E. Suero Molina, L. Stögbauer, A. Jeibmann, N. Warneke, W. Stummer, Validating a new generation filter system for visualizing 5-ALA-induced PpIX fluorescence in malignant glioma surgery: a proof of principle study, Acta Neurochir. (Wien) 162 (2020) 785–793, https://doi.org/10.1007/s00701-020-04227-7.
[29] P. Teixidor, M.Á. Arráez, G. Villalba, R. Garcia, M. Tardáguila, J.J. González, J. Rimbau, X. Vidal, E. Montané, K.L. Black, Safety and efficacy of 5-aminolevulinic acid for high grade glioma in usual clinical practice: a prospective cohort study, PLoS ONE 11 (2) (2016) e0149244.
[30] P.A. Valdés, V. Jacobs, B.T. Harris, B.C. Wilson, F. Leblond, K.D. Paulsen, D. W. Roberts, Quantitative fluorescence using 5-aminolevulinic acid-induced protoporphyrin IX biomarker as a surgical adjunct in low-grade glioma surgery, J. Neurosurg. 123 (2015) 771–780, https://doi.org/10.3171/2014.12.JNS14391.
[31] G. Widhalm, B. Kiesel, A. Woehrer, T. Traub-Weidinger, M. Preusser, C. Marosi, D. Prayer, J.A. Hainfellner, E. Knosp, S. Wolfsberger, 5-Aminolevulinic acid induced fluorescence is a powerful intraoperative marker for precise histopathological grading of gliomas with non-significant contrast-enhancement, PLoS ONE 8 (2013), e76988, https://doi.org/10.1371/journal.pone.0076988.
[32] M. Jaber, J. Wölfer, C. Ewelt, M. Holling, M. Hasselblatt, T. Niederstadt, T. Zoubi, M. Weckesser, W. Stummer, The value of 5-aminolevulinic acid in low-grade gliomas and high-grade gliomas lacking glioblastoma imaging features: an analysis based on fluorescence, magnetic resonance imaging, 18F-fluoroethyl tyrosine positron emission tomography, and tumor molecular, Neurosurgery. 78 (2016) 401–11; discussion 411. 10.1227/NEU.0000000000001020.
[33] J. Pallud, L. Capelle, L. Taillandier, M. Badoual, H. Duffau, E. Mandonnet, The silent phase of diffuse low-grade gliomas. Is it when we missed the action? Acta Neurochir. (Wien) 155 (2013) 2237–2242, https://doi.org/10.1007/s00701-013-1886-7.
[34] J. Pallud, P. Varlet, B. Devaux, S. Geha, M. Badoual, C. Deroulers, P. Page, E. Dezamis, C. Daumas-Duport, F.-X. Roux, Diffuse low-grade oligodendrogliomas extend beyond MRI-defined abnormalities, Neurology. 74 (2010) 1724 LP – 1731. 10.1212/WNL.0b013e3181e04264.
[35] M. Scherer, C. Jungk, M. Götz, P. Kickingereder, D. Reuss, M. Bendszus, K. Maier-Hein, A. Unterberg, Early postoperative delineation of residual tumor after low-grade glioma resection by probabilistic quantification of diffusion-weighted imaging, J. Neurosurg. JNS. 130 (2019) 2016–2024, https://doi.org/10.3171/2018.2.JNS172951.
[36] D.L. Phelps, J. Balog, L.F. Gildea, Z. Bodai, A. Savage, M.A. El-Bahrawy, A.V. M. Speller, F. Rosini, H. Kudo, J.S. McKenzie, R. Brown, Z. Takáts, S. Ghaem-Maghami, The surgical intelligent knife distinguishes normal, borderline and malignant gynaecological tissues using rapid evaporative ionisation mass spectrometry (REIMS), Br. J. Cancer. 118 (2018) 1349–1358, https://doi.org/10.1038/s41416-018-0048-3.
[37] J. Balog, S. Kumar, J. Alexander, O. Golf, J. Huang, T. Wiggins, N. Abbassi-Ghadi, A. Enyedi, S. Kacska, J. Kinross, G.B. Hanna, J.K. Nicholson, Z. Takats, In vivo endoscopic tissue identification by rapid evaporative ionization mass spectrometry (REIMS), Angew. Chem. Int. Ed. Engl. 54 (2015) 11059–11062, https://doi.org/10.1002/anie.201502770.
[38] O. Golf, L.J. Muirhead, A. Speller, J. Balog, N. Abbassi-Ghadi, S. Kumar, A. Mróz, K. Veselkov, Z. Takáts, XMS: cross-platform normalization method for multimodal mass spectrometric tissue profiling, J. Am. Soc. Mass Spectrom. 26 (2015) 44–54, https://doi.org/10.1007/s13361-014-0997-6.